



# 1 **The influence of glacial landscape evolution on Scandinavian** 2 **Ice Sheet dynamics and dimensions**

3 Gustav Jungdal-Olesen<sup>1</sup>, Vivi Kathrine Pedersen<sup>1</sup>, Jane Lund Andersen<sup>2</sup>, Andreas Born<sup>3</sup>

4 1) Department of Geoscience, Aarhus University, Aarhus, Denmark

5 2) Department of Physical geography, Stockholm University, Stockholm, Sweden

6 3) Department of Earth Science and Bjerknes Centre for Climate Research, University of Bergen, Bergen,  
7 Norway

8 *Correspondence to:* Gustav Jungdal-Olesen (gpo@geo.au.dk)

## 9 **Abstract**

10 The Scandinavian topography and bathymetry have been shaped by ice through numerous glacial cycles in the  
11 Quaternary. In this study, we investigate how the changing morphology has influenced the Scandinavian ice  
12 sheet (SIS) in return. We use a higher-order ice-sheet model to simulate the SIS through a glacial period on  
13 three different topographies, representing different stages of glacial landscape evolution in the Quaternary. By  
14 forcing the three experiments with the same climate conditions, we isolate the effects of a changing landscape  
15 morphology on the evolution and dynamics of the ice sheet. We find that early Quaternary glaciations in  
16 Scandinavia were limited in extent and volume by the pre-glacial bathymetry until glacial deposits filled  
17 depressions in the North Sea and build out the Norwegian shelf. From middle/late Quaternary (~0.5 Ma) the  
18 bathymetry was sufficiently filled to allow for a faster southward expansion of the ice sheet causing a relative  
19 increase in ice-sheet volume and extent. Furthermore, we show that the formation of The Norwegian Channel  
20 during recent glacial periods restricted southward ice-sheet expansion, only allowing for the ice sheet to  
21 advance into the southern North Sea close to glacial maxima. Finally, our experiments indicate that different  
22 stretches of The Norwegian Channel may have formed in distinct stages during glacial periods since ~0.5 Ma.  
23 These results highlight the importance of accounting for changes in landscape morphology through time when  
24 inferring ice-sheet history from ice-volume proxies and when interpreting climate variability from past ice-  
25 sheet extents.

26

## 27 **1 Introduction**

28 Ice holds the power to transform landscapes and constituted a major geomorphological agent in northern  
29 Europe during the Quaternary (last 2.6 Ma) where recurring glacial cycles shaped the present-day landscape.  
30 Indeed, the topography and bathymetry in and around northern Europe reveal the extensive impact of its rich  
31 glacial history, with deep fjords and U-shaped valleys attesting to the accumulated effect of widespread glacial  
32 erosion and terminal moraines indicating the extent of past ice sheets (Hughes et al., 2016). The Eurasian ice  
33 sheet complex covered much of the British Isles, all of Scandinavia, and much of northern Europe including  
34 parts of Germany, Poland, Russia, and the Baltic through multiple glacial cycles since 1 Ma (Batchelor et al.,  
35 2019). During the Last Glacial Maximum (LGM), the complex consisting of the Scandinavian ice sheet (SIS),  
36 the Barents Sea ice sheet (BSIS), and the British-Irish ice sheet (BIIS), contained an ice volume corresponding



37 to  $\sim 18.4 \pm 4.9$  m sea-level equivalent (Simms et al., 2019). On a global scale, the pace of these glacial cycles  
38 results from solar insolation variations combined with feedback mechanisms and internal dynamic effects in  
39 the climate system, in part caused by the ice sheets themselves (Hughes and Gibbard, 2018). Differences in  
40 ice volume and extent of ice sheets between glacial cycles (Fig. 1) can also be attributed to variations in  
41 moisture supply through complex global atmosphere-ocean-ice interactions (e.g., Batchelor et al., 2019;  
42 Hughes and Gibbard, 2018), with topography and proximity to the ocean being key factors determining the  
43 spatial distribution of moisture to an ice sheet. Studies on glacial landscape evolution have indicated that  
44 glacial erosion and deposition can also influence ice-sheet dynamics, ice volumes, and extent (e.g., Kessler et  
45 al., 2008; Kaplan et al., 2009; MacGregor et al., 2009; Egholm et al., 2009, 2012a,b, 2017; Anderson et al.,  
46 2012; Pedersen and Egholm, 2013; Pedersen et al., 2014; Claque et al., 2020; Mas e Braga et al., 2023). But  
47 until now, these studies have been limited to synthetic landscapes and/or limited spatial scales (smaller glaciers  
48 and ice caps). A few ice-sheet scale models are starting to consider glacial erosion (e.g., Patton et al., 2022),  
49 but the effects of long-term Quaternary landscape evolution on ice-sheet dynamics are still to be explored on  
50 a large scales for realistic landscapes and ice-sheet configurations. Understanding the influence of landscape  
51 evolution on ice-sheet dynamics requires the reconstruction of landscapes that existed prior to or at earlier  
52 stages of glacial erosion, something that can be approached using source-to-sink studies, utilizing off-shore  
53 sediment volumes of a glacial origin (e.g., Steer et al., 2012; Paxman et al. 2019; Pedersen et al., 2021).  
54



55  
56 **FIG. 1. Overview map of model domain. Maximum plausible extent of the Fennoscandian ice sheet complex**  
57 **during last glacial maximum (LGM, black line) and penultimate glacial maximum (MIS6, red dashed line)**  
58 **are overlaid (Batchelor et al., 2019) as well as the approximate location of the LGM ice divide position**  
59 **(Olsen et al., 2013).**



60

61 In this work, we focus on the well-studied Scandinavian region and investigate how the SIS may have changed  
62 its behaviour because of Quaternary landscape evolution. We use a higher-order ice-sheet model to investigate  
63 how large-scale glacial morphological features have influenced the development and dynamics of the SIS over  
64 a glacial cycle at two key times during the Quaternary: 1) before the inception of major glaciations in the  
65 beginning of the Quaternary (PREQ ~2.6 Ma) and 2) during the middle/late Quaternary (MLQ ~0.5 Ma) where  
66 major pre-glacial features in the bathymetry around Scandinavia had been filled with glacial deposits  
67 (Dowdeswell and Ottesen, 2013). Importantly, we do not intend to reconstruct realistic SIS configurations for  
68 these past time periods, but rather keep the climate forcing consistent between experiments, in order to isolate  
69 how changes in bed morphology has impacted SIS dynamics and extent. This allows us to i) explore how  
70 morphological changes can influence the dynamics, extent, and volume of the ice sheet, independent of the  
71 climatic forcing, and ii) gain insight into how ice-volume proxies could be influenced by glacial landscape  
72 evolution.

73

74 For the early Quaternary, we adopt the pre-glacial landscape reconstructions provided for the Scandinavian  
75 region by Pedersen et al. (2021) that include i) removal of glacially generated sediments offshore, ii) infilling  
76 of over-deepened fjords and glacial valleys onshore, iii) reconstruction of a wedge of older Mesozoic and  
77 Cenozoic sediments on the inner shelf that is assumed to have been eroded by glacial activity within the  
78 Quaternary (e.g., Hall et al., 2013), and finally, iv) adjustments of the landscape owing to erosion- and  
79 deposition-driven isostatic changes and dynamic topography (Pedersen et al., 2016).

80

81 In addition to this pre-glacial reconstruction, that explores an entirely different offshore bathymetry and  
82 onshore Scandinavian landscape, we also consider the more subtle effects of the large glacial trough that have  
83 been carved into the shelf bathymetry by ice streams since the middle/late Quaternary. One of the most notable  
84 of these glacio-morphological features offshore Scandinavia is the Norwegian Channel (Fig. 1). This channel  
85 is believed to have been formed by ice-stream activity sometime since 1.1 Ma (e.g., Sejrup et al. 2003), with  
86 studies suggesting that ~90 % of the deposits funneled through the channel and into the North Sea Fan were  
87 deposited within the last ~0.5 Ma (Hjelstuen et al., 2012). Recently, it has been suggested that the channel  
88 formed mostly within the last ~0.35 Ma (Løseth et al., 2022). An erosional unconformity at the base of the  
89 channel is draped by post-LGM sediments, suggesting that the channel experienced erosion within the last  
90 glacial cycle (Hjelstuen et al., 2012). For the last glacial cycle, it has been proposed that the Norwegian  
91 Channel Ice Stream (NCIS) was active in stages but mainly during the LGM (e.g., Sejrup et al., 1998; Sejrup  
92 et al., 2003). Ice streaming in the outer parts of the channel near the shelf break started close to the LGM with  
93 increased activity promoting ice retreat around 19 ka BP because of the increased ice mass loss (Sejrup et al.,  
94 2016). The retreat translated southwards over time as the SIS unzipped from the adjacent BIIS after which  
95 with ice streaming was mostly confined to the main trunk of the channel (Sejrup et al., 2016).

96

97 **2 Methods**



98 For the numerical experiments presented in this study, we use the depth-integrated second-order shallow-ice  
99 approximation iSOSIA (Egholm et al., 2011, 2012a,b). We conduct our experiments by simulating a full glacial  
100 cycle of 120 ka on different topographies. In the following section we will present the numerical model, the  
101 model setup, and the experimental design.

102

### 103 **2.1 Modelling the Scandinavian Ice Sheet**

104 The ice flow in iSOSIA is governed by a second-order approximation of the equations for Stokes flow (e.g.,  
105 Egholm et al., 2011). The velocities are depth integrated to yield a 2D one layer ice model, implemented here  
106 using a regular grid (e.g., Egholm and Nielsen, 2010). The second-order nature of the approximation ensures  
107 that ice velocities depend non-linearly on ice thickness, ice-surface gradients, as well as longitudinal and  
108 transversal horizontal stress gradients (Egholm et al., 2011, 2012b). Details on the iSOSIA model, including  
109 the importance of the higher order ice dynamics involved, have been described in depth elsewhere (Egholm  
110 and Nielsen, 2010; Egholm et al., 2011, 2012a,b).

111

112 The depth-integrated ice-creep velocity is calculated using temperature-dependent Glen's flow with a stress  
113 exponent,  $n$ , equal to 3:

114

$$115 \quad \varepsilon_{ij} = A_{flow} \tau_e^{n-1} s_{ij},$$

116

117 where  $\varepsilon$  is the strain rate tensor,  $ij$  denoting the components of the tensor,  $A$  is the ice flow parameter,  $\tau_e$  is the  
118 effective stress and  $s$  is the deviatoric stress tensor (Egholm et al., 2011). A simple Weertman sliding scheme  
119 is used to calculate the contribution of basal sliding to depth-integrated ice velocities:

$$120 \quad u_b = A_{sliding} \frac{t_s^3}{N},$$

121

122 where  $u_b$  is the basal velocity,  $A_{sliding}$  is an ice sliding coefficient,  $t_s$  is the bed parallel shear stress and  $N$   
123 is the effective pressure at the base (Egholm et al. 2011).  $A_{sliding}$  is chosen to give realistic sliding in the order  
124 of several hundred meters per year for example in fjords or near the shelf edge in the Norwegian Sea, similar  
125 to surface velocities in comparable areas of modern-day ice-bodies (e.g., Millan et al. 2022). To allow for  
126 faster ice flow for soft bed subglacial conditions (e.g., Gladstone et al., 2020, Han et al., 2021),  $A_{sliding}$  is  
127 enhanced by a factor of 5 in offshore regions and onshore in northern Europe where thick soft sediments cover  
128 the bed.

129

130

131

132 In this study, we focus on grounded ice only, as ice-shelf dynamics are computationally expensive to resolve  
133 on the timescales of our experiment and because constraints on ice shelf extent in middle or early Quaternary  
134 glaciations are sparse due to a lack of reliable dates on submarine landforms (e.g., Jakobsson et al. 2016).  
135 Some older studies suggest that an ice shelf was present during recent glaciations in the North Atlantic and



136 Arctic regions (Hughes et al. 1977, Lindstrom et al. 1986). However, while ice shelf stability is sensitive to  
 137 bathymetric configurations (Bart et al. 2016) and is a deciding factor in grounding line migration, we limit our  
 138 focus here to large-scale morphological features, such as the Norwegian Channel, created by an ice stream in  
 139 contact with the sea bed (Sejrup et al., 2016). Consequently, we do not consider floating ice in our simulations  
 140 and remove floating ice by introducing a fast melt rate for ice that does not meet the grounding criterion:

$$141 \quad H_{ice} > (SL + H_{ice}) \frac{\rho_{water}}{\rho_{ice}},$$

142 where  $H_{ice}$  is ice thickness,  $SL$  is local sea level and  $\rho_{water}$  and  $\rho_{ice}$  are the densities of water and ice, respectively.  
 143 Special boundary conditions are employed at the approximate locations where the SIS meets the BSIS and  
 144 BISS by introducing an ‘ice wall’ where the ice flux is zero to emulate divergent ice flow when these ice sheets  
 145 merge during glacial maxima. At the edges of the model domain, we employ open boundary conditions to  
 146 allow for ice to flow out of the domain. Common model parameters are presented in Table 1.

147

Parameter		Value	Unit
$\rho_{ice}$	Ice density	910	kg m <sup>-3</sup>
$q_b$	Geothermal heat flux	0.045	W m <sup>-2</sup>
$L_i$	Latent heat of ice	334	kJ kg <sup>-1</sup>
$A_{flow}$	Ice flow parameter	$1.5 \cdot 10^{-15}$	Pa <sup>-3</sup> y <sup>-1</sup>
$A_{sliding}$	Ice sliding parameter	0.4	m Pa <sup>2</sup> y <sup>-1</sup>
$n$	Ice flow exponent	3	
$f_{flow\ enhancement}$	Ice flow enhancement factor	100	
$m$	Ice sliding exponent	3	
$F_{sliding\ enhancement}$	Sliding enhancement factor offshore	5	
$mPDD$	PDD factor	0.005	m °C <sup>-1</sup> d <sup>-1</sup>
$SL$	Mean sea level	[0 : -130]	m
$dT_h$	Lapse rate	6.5	°C km <sup>-1</sup>
$dT_{m,e}$	Easterly temperature gradient	$[-1.3 : -2.3] \cdot 10^{-6}$	°C m <sup>-1</sup>
$dT_{m,n}$	Northerly temperature gradient	$[-3.5 : -10] \cdot 10^{-6}$	°C m <sup>-1</sup>
$dA_{T,e}$	Easterly annual temperature variation gradient	$[7.8 : 0.11] \cdot 10^{-6}$	°C m <sup>-1</sup>
$dA_{T,n}$	Northerly annual temperature variation gradient	$[2.0 : 1.4] \cdot 10^{-6}$	°C m <sup>-1</sup>
$dP/dT$	Change in precipitation with change in temperature	0.029	°C <sup>-1</sup>
$D_L$	Thickness of elastic lithosphere	50	km

148

149

150

151 **TABLE 1. Common parameters in the ice sheet model and mass balance scheme. Numbers in brackets**

152 **denote min and max values.**

153



154 **2.1.1 Mass balance**

155 In the simulations we present here, we assume that the mass balance ( $\dot{M}_{ice}$ ) of the ice sheet can be  
156 approximated using three components:

157 
$$\dot{M}_{ice} = \dot{m}_{acc} - \dot{m}_s - \dot{m}_b,$$

158 where  $\dot{m}_{acc}$  is the rate of accumulation,  $\dot{m}_s$  is the surface melt rate and  $\dot{m}_b$  is the basal melt rate (Egholm et  
159 al. 2012b). We use a positive-degree-day (PDD) model to estimate accumulation rate and surface melt rate as  
160 a function of mean annual temperature, annual temperature variation, and mean annual precipitation at every  
161 point in our model domain for every time step (e.g., Magrani et al., 2022).

162 The yearly temperature variation in a given cell, is approximated by a sine function based on the mean annual  
163 temperature and annual temperature amplitude (see below). The melt rate in m/yr is calculated in the PDD  
164 model as:

165 
$$\dot{m}_s = m_{PDD} \sum_{n=1}^{365} T_{positive}$$

166 where  $m_{PDD}$  is the positive-degree-day factor multiplied with the sum of positive degrees each year. Here, we  
167 consider a single melting degree factor for both ice and snow, since all precipitation is turned into ice after  
168 accumulation (based on yearly average rates). The accumulation rate is approximated by:

169 
$$\dot{m}_{acc} = \frac{n_{frost}}{365} \cdot P,$$

171 where  $n_{frost}$  is the number of days with negative temperatures in a year and  $P$  is the annual precipitation. The  
172 temperature forcing that drives spatial and temporal changes in mass balance in our simulations is based on  
173 mean temperature, annual temperature amplitude, and lapse rate that vary across the model domain using  
174 spatial gradients that vary in time. Two climate states are chosen to represent the extremes of our model: a  
175 glacial maximum state and an interglacial state, and the spatial gradients of the full glacial cycle of our model  
176 simulations are subsequently defined to vary in between these extremes using a glacial index that resembles  
177 the normalized LR04 Benthic Stack (Lisiecki and Raymo, 2005) with glacial maximum in this climate forcing  
178 occurring at 18 ka BP. Here we define spatial ( $x, y, z$ ) gradients at the glacial maximum using multiple linear  
179 regression on MPI-ESM climate model outputs (LGM experiment; Jungclaus et al. 2019). For the interglacial  
180 state we define spatial gradients using the ERA-interim reanalysis data for modern day (Dee et al. 2022).  
181 Finally, the lapse rate was found to be close to constant, so we keep this fixed at  $6.5 \text{ }^\circ\text{C km}^{-1}$ . With this  
182 approach, the temporally-varying temperature forcing of the entire grid can be defined from a single grid cell  
183 in the lower left corner and still capture a coastal-continental (east-west) gradient, a polar gradient (south-  
184 north), and an altitudinal gradient (lapse rate) in temperature. However, we cannot capture local effects that  
185 arise from changes in complex atmospheric circulations patterns over time that might have important  
186 implications for glacial dynamics and ice extent (e.g., Liakka et al. 2016, Hughes and Gibbard, 2018).

187

188 To represent precipitation in our simulations, we use a climate-corrected modern-day mean precipitation field  
189 (Pendergrass et al., 2022), modulating the local precipitation in every grid cell using the following equation:



190

$$P = P_0 \cdot e^{kTp \cdot \Delta T},$$

191

where  $P_0$  is the local modern day (interglacial) precipitation,  $\Delta T$  is the change in temperature in a cell from the previous time step, and  $kTp$  represent the rate of change in precipitation for a change in temperature with a value of  $0.029 \text{ } ^\circ\text{C}^{-1}$ . The value of  $kTp$  is found by optimization through a comparison between mean precipitation at LGM in MPI-ESM and mean precipitation in the modern-day ERA-interim data set. By scaling the precipitation with changes in temperature we can capture some of the effects an ice sheet will impose on moisture supply, by limiting snow fall in the central parts of the ice sheet (Fig. 3D).

197

198

Basal melting rate is calculated as the difference between of geothermal heat flux from the bed and the heat flux from the temperature gradient in the basal ice (Egholm et al., 2012a):

199

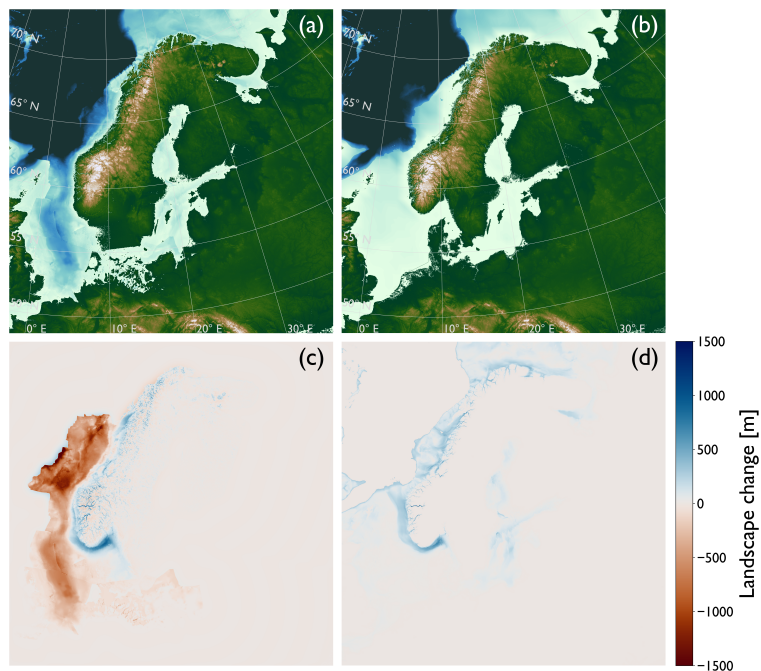
200

$$\dot{m}_b = \frac{q_b - q_c}{\rho_{ice} L_i},$$

201

where  $L_i$  is the latent heat for fusion of ice and  $\rho_{ice}$  is the density of ice (Tab. 1).

202



203

204

**FIG. 2. Paleo-topographic and bathymetric reconstructions. a) the PREQ experiment, b) the MLQ experiment, c) and d) show the differences between the panel above and the modern-day topography and bathymetry.**

206

207

208

209



### 210 **2.1.2 Topography and bathymetry**

211 The focus of this study is to examine the influence of bed topography on ice sheet behaviour, exemplified by  
212 simulating the SIS on landscape configurations representing different periods in the Quaternary. For  
213 comparison, we simulate the SIS on modern-day topography and bathymetry over the last glacial cycle in a  
214 reference model. The reference experiment uses the global DEM GEBCO 2022 (GEBCO Bathymetric  
215 Compilation Group., 2022) global grid sampled at 10 km x 10 km for the ice model (the same grid resolution  
216 is used in all experiments). Because of computational limitations, a model resolution higher than 10 km is not  
217 feasible. Having a higher resolution would allow us to resolve glacial morphology in higher detail and could  
218 lead to interesting findings regarding the influence of fjord systems in western Norway on ice sheet dynamics.  
219 Here, we focus on larger features such as the Norwegian Channel where a 10 km resolution is sufficient.  
220 Throughout the model simulations, ice-driven isostasy is handled with a two-dimensional uniform thin elastic  
221 plate model (e.g., Pedersen et al. 2014).

222

223 The pre-glacial landscape is adopted from Pedersen et al. (2021) and reconstructed using a source-to-sink  
224 approach that also considers i) a component of glacial erosion that has taken place on the inner shelf, ii)  
225 erosion-driven isostasy, and iii) a component of dynamic topography (Pedersen et al., 2016). For further details  
226 on the approach see Pedersen et al. (2021). Here, we extend these previous reconstructions and remove the  
227 Quaternary sediment package from all sectors of the North Sea, to reconstruct a realistic pre-glacial bathymetry  
228 for the entire region (Binzer et al., 1994; Rise et al., 2005; Nielsen et al., 2008; Gołędowski et al., 2012; Lamb  
229 et al. 2018; The Southern Permian Basin Atlas). These additional sediment volumes, from outside of the  
230 Norwegian and Danish sectors, are not included in the landscape reconstruction onshore Scandinavia. The  
231 result is a landscape representing a pre-glacial state before any major glaciations in Scandinavia, featuring a  
232 large submarine depression in the North Sea and a much narrower continental shelf along the Norwegian  
233 margin than at present (Fig. 2a,c). In addition to the PREQ experiment two sub-experiments are presented:  
234 ‘PREQ-onshore’ where only the onshore fjord erosion has been reconstructed (material added compared to  
235 present-day) and ‘PREQ-offshore’ where only the offshore deposition has been reconstructed (material  
236 removed compared to present-day). Neither of these additional sub-experiments considers the offshore  
237 sediment wedge on the shelf. With the sub-experiments we can assess which processes control the behaviours  
238 and ice volume changes observed in the PREQ experiment.

239

240 For the middle/late Quaternary (MLQ) experiment, we reconstruct the bathymetry by estimating the volumes  
241 of erosion that have been carved into the modern day sea-bed by ice streams on the Norwegian shelf and in  
242 the Norwegian Channel (Fig. 1). This bathymetric erosion is estimated using the geophysical relief method  
243 (e.g., Steer et al., 2012; Pedersen et al., 2021) on the present-day GEBCO 2022 global DEM (GEBCO  
244 Bathymetric Compilation Group., 2022), using a grid resolution of 1 x 1 km and a sliding window radius of  
245 35 km. The resulting filled bathymetry, that also fills fjords to sea level, is adjusted with the flexural isostatic  
246 response to loading using gFlex 1.1.1 (Wickert, 2016) with an effective elastic thickness of 15 km. This  
247 reconstruction of the Scandinavian morphology is meant to represent a state before the formation of the





248 Norwegian Channel (Fig. 2b,d) and could represent an age of approximately ~0.5 Ma. This approximate age  
249 is supported by the presence of buried mega-scale glacial lineations and drumlins in stratigraphic sequences  
250 of the North Sea suggesting that grounded ice has been present since ~0.5 Ma, whereas the lack of these  
251 features in the older strata indicate that early Quaternary glaciations did not ground, but only supplied icebergs  
252 to the North Sea (Dowdeswell and Ottesen, 2013; Rea et al., 2018).

253

### 254 **3 Results**

255 In this section we start by presenting the results from our reference model simulating the evolution of the SIS  
256 on the present-day topography and bathymetry over the last glacial period. Then we present the results of our  
257 two experiments with reconstructed topography and bathymetry and how they differ from the reference model.  
258 Lastly, we present our findings regarding a possible timing of formation for the Norwegian Channel.

259

260

261

262

263

264

265

266

267

268

269

270

271

272

273

274

275

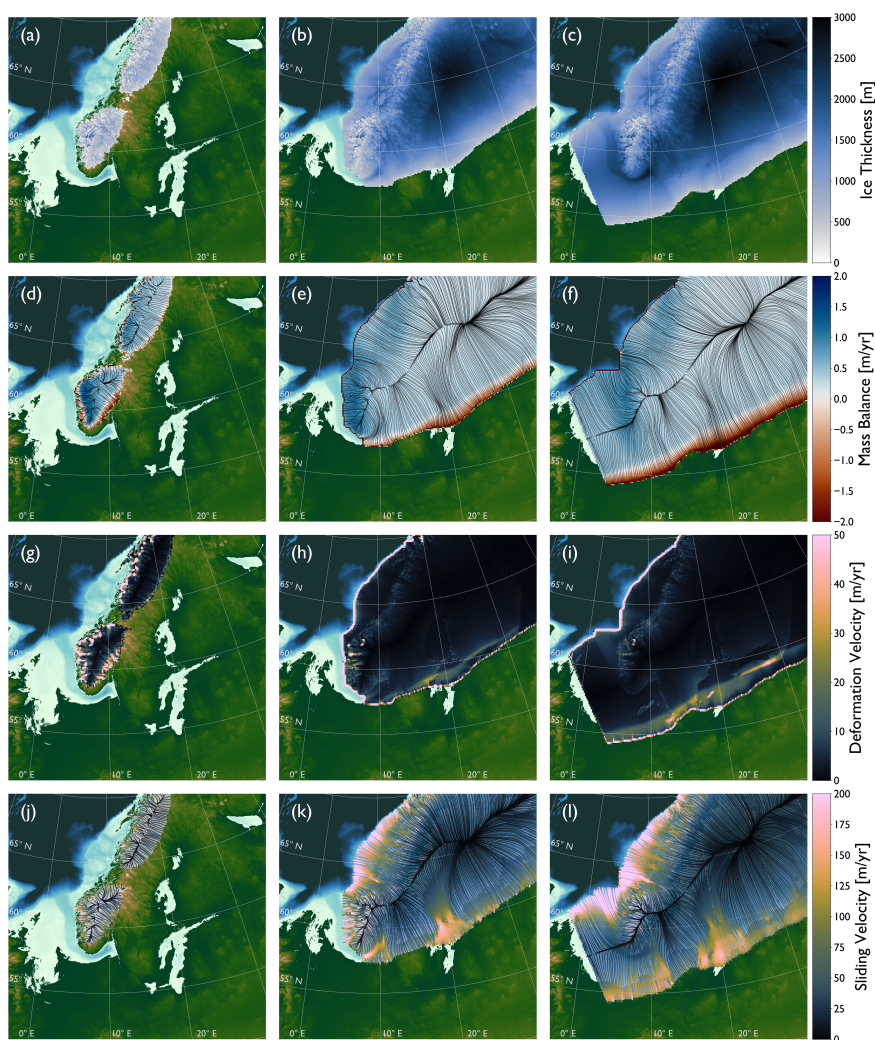
276

277



278

279



280

281 **FIG. 3.** Model output from three time slices of the reference experiment, left column: early glaciation (72  
282 ka), middle column: late-intermediate glaciation (22 ka), right column: glacial maximum (17 ka). a-c) ice  
283 thickness, d-f) mass balance, g-i) depth averaged deformation velocity and j-l) sliding velocity.

284

285

286

287

288



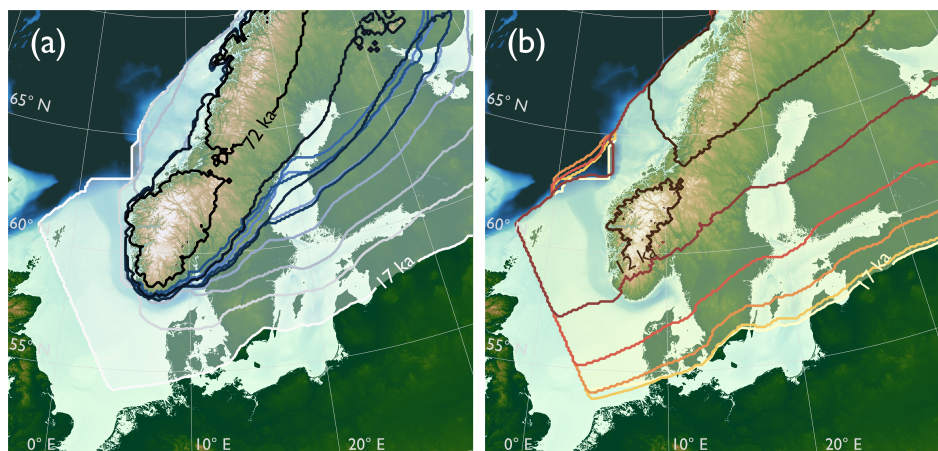
289

### 290 **3.1 Reference model**

291 To illustrate the spatial and temporal development of the SIS in our model simulations, we present model  
292 output from three snapshots in time (Fig. 3): minor ice build-up during early glaciation (72 ka), moderate  
293 glacial build-up during intermediate times of the glaciation (22 ka), and glacial maximum that happens in these  
294 simulations at 17 ka. We note that the delayed glacial maximum timing in our models compared to the timing  
295 of the reconstructed maximum extent in Scandinavia (~21-19 ka, Hughes et al., 2016) is a direct consequence  
296 of the chosen climate forcing, utilizing a glaciation index that peaks at 18 ka. We do not intend here to match  
297 the exact timing of the maximum extent (LGM). During our simulated early glaciation, ice extent is limited to  
298 mountain regions with high topography and high latitude regions in Norway and Sweden (Fig. 3a). Mass  
299 balance is positive ~1.5 m/yr in high altitude regions at the Norwegian coast where precipitation is high, and  
300 temperatures are low (Fig. 3d). Ice deformation and sliding is high up to >50 m/yr and >200 m/yr respectively,  
301 during early glaciation (Fig. 3g,j), where ice is thin and controlled by the underlying topography that includes  
302 mountainous regions dissected by fjords and valleys. During the intermediate glaciation, the ice sheet has  
303 advanced onto the shelf region, with grounded ice on the Norwegian margin, and the ice sheet has started to  
304 advance into the North Sea through the inner part of the Norwegian Channel (Fig. 3b). The mass balance  
305 reaches ~1 m/yr at the west coast of Norway (Fig. 3e), with values across most of the ice sheet <0.5 m/yr, and  
306 negative mass balance at the south/western margin reaching ~-2 m/yr where the ice is thin and velocities exceed  
307 ~200 m/yr (Fig. 3h,k). Along the coastal margin to the west, the mass balance is negative in a narrow zone  
308 where floating ice is melting fast. Sliding is notably high, reaching >200 m/yr in the inner parts of the  
309 Norwegian Channel (Fig. 3k). The ice flow is still steered by topography in the high regions of Southern  
310 Norway, and also in the Bothnic Bay, whereas the main divide in Northern Scandinavia has shifted east, being  
311 largely independent of the underlying topography (Fig. 3c). During glacial maximum, the ice sheet reaches a  
312 thickness of >3000 m in the central parts (Fig. 3c) with a relatively low positive mass balance along the west  
313 coast of Norway (<1 m/yr; Fig. 3f) with the same general spatial pattern in accumulation and ablation as the  
314 intermediate glaciation (Fig. 3e) across the ice sheet as during the intermediate glaciation. Sliding is high along  
315 the northeastern margin of the ice sheet (>200 m/yr) especially near the shelf break where ice is funnelled  
316 towards the deeper ocean (Fig. 3l). For a while (~5,000 yrs) during the maximum expansion, the ice sheet  
317 merges with the BIIS in the western part of the North Sea, simulated as an ice wall (Fig. 3f,l). At this time, the  
318 ice flow rearranges into a divergent pattern from the ice saddle that emerges between the BIIS and the SIS.  
319 Consequently, the ice flows across the Norwegian Channel during the maximum extent of the ice sheet instead  
320 of being focused in the channel itself, as the ice is diverged southward, driven by the surface slope of the ice  
321 sheet under this ice configuration (Fig. 3l). It is worth noting that the reference model captures a realistic  
322 placement of the LGM ice divide (Fig. 3f) in accordance with geological observations (Fig. 1; Olsen et al.,  
323 2013). The glacial maximum ice extent in our reference experiment is within the maximum LGM ice extent  
324 (Fig. 1; Hughes et al., 2016), albeit with less ice towards the southern margin and more ice in northeast.

325

326



327

328 **FIG. 4. Advance and retreat of the SIS in the reference experiment. A) ice advance in 5 kyr intervals between**  
329 **model years 72 ka and 17 ka. B) retreat in 1 kyr intervals from 17 to 12 ka.**

330

331 Buildup of the SIS from early mountain glaciation to glacial maximum happens gradually with grounded ice  
332 on the Norwegian shelf forming 10,000 model years before glacial maximum, and ice advance in the North  
333 Sea occur over just 5000 model years approaching glacial maximum extent (Fig. 4A). In contrast, the ice  
334 retreat is rapid with ice mass loss from the glacial maximum back to a state similar to early glaciation  
335 happening over just 5000 model years (Fig. 4B).

336

337

338

339

340

341

342

343

344

345

346

347

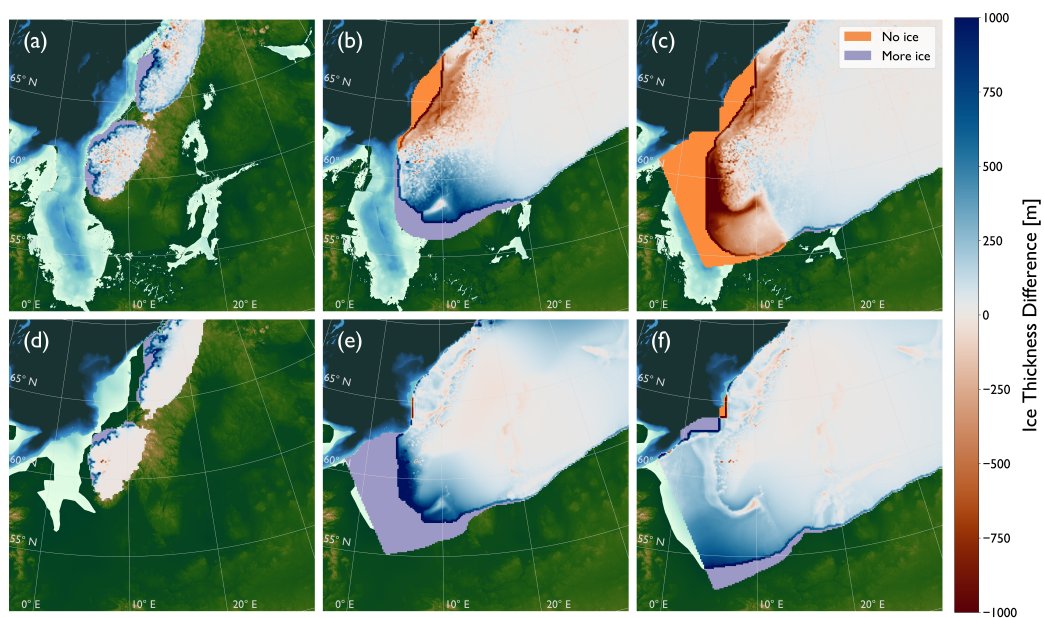
348

349

350

351

352



353

354 *FIG. 5. Differences in ice thickness for the a,b,c) PREQ and d,e,f) MLQ experiments compared to the*  
355 *reference experiment for the same time slices as Fig. 3. Blue colors means more ice in this experiment than*  
356 *the reference experiment and red colors means less ice.*

357

358

359

360

361

362

363

364

365

366

367

368

369

370

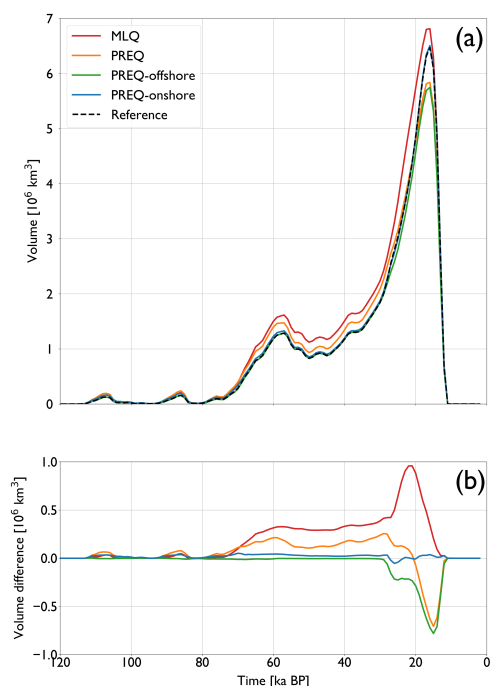
371

372

373

374

375



376

377 **FIG. 6. a) ice volume over time for the different experiments, b) volume differences between the different**  
 378 **experiments and the reference experiment.**

379

### 380 3.2 Results from PREQ and MLQ

381 In the model simulation representing ice-sheet behavior on an early Quaternary landscape morphology (PREQ;  
 382 Fig. 2a, Fig. 5a-c), the ice sheet initially extends further than the reference model (Fig. 5a, purple color),  
 383 particularly towards the Norwegian coast. At the intermediate stage (Fig. 5b), the ice sheet shows a smaller  
 384 extent and thickness towards the Norwegian margin (Fig. 5b, orange color), whereas the ice extends further  
 385 towards the south (Fig. 5b, purple color) with an ice thickness increase of >500 m in some regions. The location  
 386 of the present-day Norwegian Channel shows a much thinner ice since this bathymetric depression is not  
 387 present in the PREQ landscape reconstruction (Fig. 5b). At the maximum extent, the ice sheet is smaller both  
 388 along the western and the southwestern margins (Fig. 5c, orange color), with a general decrease in ice sheet  
 389 thickness (Fig. 5c, red colors). The reduced extent and ice volume during the maximum extent result in ~10 %  
 390 lower maximum ice volume than the reference model (Fig. 6, orange curve). The large difference in ice volume  
 391 between the PREQ experiment and the reference experiment is largely driven by differences in bathymetry  
 392 (PREQ-offshore; Fig. 6a, green curve) as changes in topography do not lead to significant differences in ice  
 393 volume compared to the reference model (PREQ-onshore, Fig. 6a, blue line)

394

395



396 For the MLQ simulation that represents ice flow on a landscape morphology that existed prior to extensive  
397 erosion of the bathymetry by ice streaming (Fig. 2b, Fig. 5d-f), the ice sheet also starts slightly larger (Fig. 5d,  
398 purple color) compared to the reference model. At the intermediate stage, the ice sheet has already extended  
399 all the way across the North Sea (Fig. 5e, purple color), showing also a significantly thicker ice sheet in the  
400 adjoining regions onshore Scandinavia. This trend is continued during the maximum extent, where the MLQ  
401 ice sheet extends even further, particularly towards the south (Fig. 5f, purple colors). In general, the extent of  
402 the MLQ ice sheet is not changed along the Norwegian margin, where the width of the shelf has not changed  
403 for this simulation (Fig. 5e-f). The increased ice extent and ice thickness in the MLQ simulation result in a  
404 maximum ice volume that is ~25 % more than the reference model during intermediate stage and ~5 % during  
405 the glacial maximum as a direct result of the changed bathymetry (Fig. 6, red line).

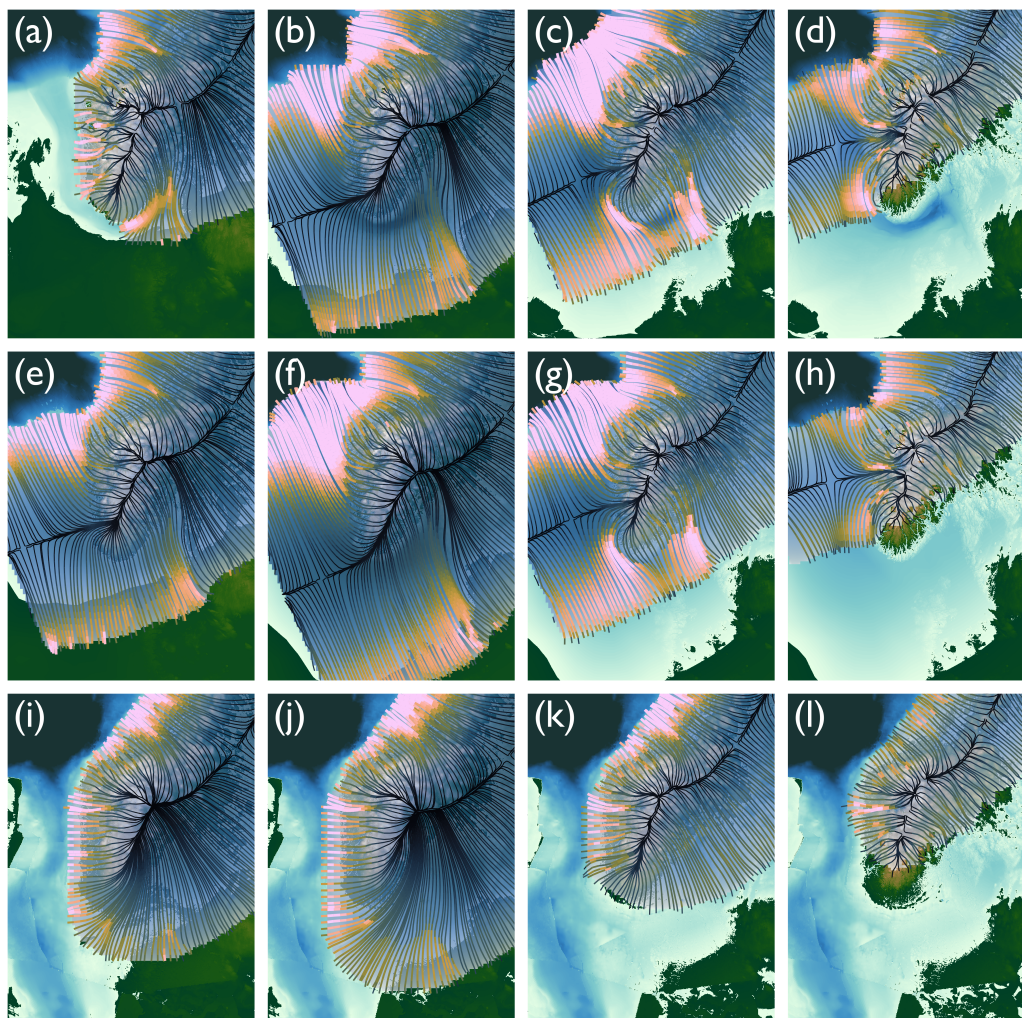
406

### 407 3.3 Sliding in the Norwegian Channel

408 The erosive power of ice is a product of ice flux over a region with grounded ice (Patton et al. 2022) and is  
409 strongly correlated with ice sliding velocity (Cook et al. 2020), which means sliding velocity can be considered  
410 a proxy for erosive potential. Here we explore whether our higher-order ice-sheet model can capture the erosive  
411 potential through sliding in the Norwegian Channel in the present-day bathymetry of the reference model and  
412 whether the model can predict erosion when the channel is not there in the PREQ and MLQ experiments. The  
413 ice dynamics in our reference simulation show significant sliding in the Norwegian Channel in four distinct  
414 phases (Fig. 7a-d). In the early glacial stage, the ice is sliding fast southeast of southern Norway along the  
415 deepest part of the channel (Fig. 7a). As the ice approaches maximum extent, the sliding pattern changes  
416 because of the different ice flow patterns that arise as an ice saddle emerges in the North Sea when the SIS  
417 merges with the BIIS (Fig. 7b). At this stage, ice flows south across the channel from the southern mountains  
418 of Norway, following the steepest surface gradient of the ice sheet. Instead, sliding is now mostly concentrated  
419 in the outer parts of the Norwegian Channel close to the North Sea Fan (Fig. 7b). During retreat, ice sliding  
420 continues in the outer parts of the channel, but also becomes prominent along the southern tip of Norway with  
421 ice sliding towards the southeast, and in the inner parts of the channel near Oslo Fjord (Fig. 7c). Finally, as the  
422 ice sheet retreats further, continued sliding toward the North Sea Fan is complemented by a phase of southward  
423 sliding in the channel along the south-western coast, a region that had not seen significant prior sliding (Fig.  
424 7d). In figure 7e-h we show the same time slices for the MLQ experiment. Here, the ice extends further towards  
425 the west and has already formed a saddle between the SIS and the BIIS during the initial phase of the glacial  
426 cycle (Fig. 7e), and sliding is high towards the shelf break in the region that will later become the outermost  
427 part of the Norwegian Channel. Sliding velocities towards the shelf break are consistently high throughout the  
428 model simulation (Fig. 7f,h), whereas sliding accelerates in the inner parts of what will become the Norwegian  
429 Channel during ice retreat (Fig. 7g). In the last time slice, sliding velocity is lower than the reference  
430 experiment but has the same general pattern (Fig. 7h), with sliding in some regions along the west coast of  
431 Southern Norway. In figure 7i-l we present the time slices for the PREQ experiment. Across all four panels  
432 the patterns differ from the reference and MLQ experiments. Instead, we observe high sliding velocities



433 towards the west across where the channel is today (Fig. 7i-k). In the last time slice we observe very little  
434 sliding as the ice has retreated mostly onshore at this time in the PREQ experiment (Fig. 7l).  
435  
436  
437



438  
439  
440 **FIG. 7. Sliding velocity in southwestern Norway for reference model year a) 23 ka, b) 17 ka, c) 14 ka, and**  
441 **(d) 13 ka. Same color scale as Fig. 3j-l. Same for MLQ experiment e-h and PREQ experiment i-l.**  
442  
443  
444





445 **4. Discussion**

446 **4.1 Ice extent and volume**

447 The volume of ice contained in the Scandinavian ice sheet at LGM is estimated to be between 5.3-6.5  $10^6$  km<sup>3</sup>  
448 (Hughes et al. 2016). This is in good agreement with our reference experiment that reaches 6.5 M km<sup>3</sup> at glacial  
449 maximum. The ice divide of the SIS in the reference experiment is in good agreement with observations (Fig.  
450 1, Fig. 3f) which also affirms that our model captures an adequate representation of the ice sheet during the  
451 last glacial period. The differences in maximum ice extent between our reference experiment and observations  
452 (Hughes et al., 2016; Fig. 1) can be attributed to the simple mass balance implemented in our model using  
453 linear gradients that does not capture the complex nature of the regional climate during the last glacial cycle  
454 but is an adequate approximation for our purposes. Geological observations suggest that the main ice advance  
455 in Denmark approaching glacial maximum between 20-22 ka came from the northeast bringing till deposits of  
456 Middle Swedish provenance (Houmark-Nielsen, 2004), whereas the main ice advance into Denmark in our  
457 reference experiment comes from the north (Fig. 4a). A possible reason that our model does not capture this  
458 dynamic in the southerly ice advance could be the lack of subglacial hydrology in the model which can increase  
459 sliding rates (Egholm et al. 2012a). It could also be the lack of a more complex stress dependent ice viscosity,  
460 where the Glen's flow law stress exponent can increase to  $n \approx 4$  in some areas, which can increase the flow  
461 velocity by an order of magnitude (Millstein et al., 2022). These effects could be important especially in the  
462 southern parts of the ice sheet where the ice is thin and fast flowing during advance (Fig. 3c,i). Here, an even  
463 faster and thinner ice might be more sensitive to the low relief topography of southern Scandinavia leading to  
464 a more westerly ice flow from Sweden into Denmark in agreement with the observations.

465

466 We cannot directly compare the ice extents in our experiments with reconstructions of past SIS extent as we  
467 use the same climate forcing between experiments, but we can assess whether differences in past ice sheet  
468 extents follow the same trends as we see in this study that is based solely on differences in morphology.  
469 Batchelor et al. (2019) use empirical data to evaluate past northern hemisphere glacial extents, and suggest  
470 best-estimate maximum southern extents of the MIS 12 (429-477 ka), MIS 16 (622-677 ka), and MIS 20-24  
471 (790-928 ka) ice sheets to be somewhere between the best-estimate maximum MIS 6 extent and the LGM  
472 extent (Fig. 1; dashed red line, black line, 132-190 ka), although the MIS 16 and MIS 20-24 maximum ice  
473 sheet extents are highly uncertain. These reconstructions are based on very limited observations and in some  
474 cases (e.g., MIS 12 and 16) the estimates are mostly based on similarities in the  $\delta^{18}\text{O}$  curve (Batchelor et al.,  
475 2019). We show with this study that purely morphological differences in bathymetry between the last glacial  
476 period and  $\sim 0.5$  Ma ka (MLQ experiment, similar in time to MIS 12/16) allow for larger ice-sheet extents  
477 simply owing to geomorphic changes during this time period. This suggests that both climatic and topographic  
478 forcing might have caused these (possibly) large ice extents of the mid-late Quaternary (MIS 12,16,20-24).  
479 Indeed, our results showcase that a smooth bathymetry in the North Sea region (i.e., lacking glacial  
480 morphology), such as before the inception of the Norwegian Channel, could lead to earlier and more extensive  
481 southerly ice advance within a glacial period (Fig. 5e). On the other hand, our simulation of early Quaternary  
482 glaciations suggests that ice buildup across the North Sea was not plausible at this early stage of glacial



483 landscape evolution. Indeed, in the PREQ experiment we find that the SIS could extend no further than the  
484 continental shelf during the early Quaternary (Fig. 5b,c). This is consistent with a study of buried glacial  
485 landforms in the central North Sea documenting ice-berg plough marks in early Quaternary sediments  
486 (Dowdeswell et al., 2013). Our reconstructed early Quaternary ice sheet would have supplied icebergs that  
487 created these plough marks.

488

489 The differences we find in ice volume at the maximum glacial extent (~5 % higher for MLQ, ~10 % lower for  
490 PREQ), illustrate how differences in morphology affects ice volume independent of the climate forcing. This  
491 has implications for the proxies we use for ice volume history. Looking at the peak values in the LR04 Benthic  
492 Stack for LGM ( $5.02 \pm 0.03 \text{ ‰}$ ), MIS 6 ( $4.98 \pm 0.05 \text{ ‰}$ ), MIS 12 ( $5.08 \pm 0.05 \text{ ‰}$ ), MIS 16 ( $5.08 \pm 0.06 \text{ ‰}$ ),  
493 and MIS 20-24 ( $4.69 \pm 0.08 \text{ ‰}$ ), the proportional differences between these  $\delta^{18}\text{O}$  peaks (~1-7 %) are less than  
494 the proportional differences of 5-10% in peak ice volume between the model simulations presented here,  
495 suggesting that landscape evolution can play an important role in controlling ice volume. Clearly the effect of  
496 glacial morphology is local whereas the LR04 Benthic Stack is a global proxy and in addition, local ice volume  
497 also depend on global atmospheric circulation patterns which can lead to asynchronous development of the ice  
498 sheets during a glacial period (e.g., Liakka et al., 2016) that will also influence ice-sheet volume between  
499 glacial cycles. Nevertheless, according to this study landscape morphology alone can account for ~10 % (~25  
500 % during ice build-up) difference in ice volume between glacial cycles for the Scandinavian region implying  
501 that glacial landscape evolution could be an overlooked mechanism impacting global ice volume and thereby  
502  $\delta^{18}\text{O}$  values.

503

#### 504 **4.2 Formation of the Norwegian Channel**

505 It is uncertain how and when the Norwegian Channel was formed, with studies estimating the time of formation  
506 to be between 0.35-1.1 Ma – with more recent studies suggesting younger ages (e.g., Sejrup et al., 2003;  
507 Hjelstuen et al., 2012; Løseth et al., 2022). In this study, we have assumed that the entirety of the Norwegian  
508 Channel formed after 0.5 Ma (MLQ).

509

510 A previous modelling study suggests that the NCIS was active in stages with streaming in the inner parts of  
511 the channel leading up to, and deactivated during, glacial maximum because of the saddle forming from the  
512 merging of the BIIS and the SIS (Boulton and Hagdorn, 2006). In that study, the NCIS was mostly active near  
513 the shelf break at LGM and during retreat the ice stream funnelled ice along the entire length of the Norwegian  
514 Channel (Boulton and Hagdorn, 2006). We find in this study, that ice streaming was active in the inner parts  
515 of the channel before the saddle formed between the BIIS and the SIS, after which ice streaming velocity  
516 increased dramatically in the outer parts of the Norwegian Channel near the shelf break and mostly deactivated  
517 in the inner parts of the Norwegian Channel, consistent with other literature based on observations of e.g.  
518 subglacial landforms combined with dated sediment cores (Sejrup et al., 2016). However, our reference  
519 experiment does not mimic at any time an NCIS spanning the entire trunk of the Norwegian Channel, which  
520 would significantly contribute to ice mass loss from rapid grounding line retreat as is supported by observations



521 (Sejrup et al., 2016). We cannot with this model setup rule out the occurrence of continuous ice streaming in  
522 the entire Norwegian Channel after the LGM. Indeed, some processes central to reproducing realistic ice  
523 stream behaviour is not included in iSOSIA, including enhanced basal melt owing to basal friction, leading to  
524 accelerated thinning in regions with rapid ice sliding as well as effects of internal friction and temperature on  
525 ice viscosity which can greatly amplify sliding velocities (Millstein et al., 2022; Bondzio et al., 2016). These  
526 mechanisms could contribute to highly elevated sliding velocities, especially in the NCIS, and could facilitate  
527 a propagation of the streaming activity in the outer parts of the channel to the inner parts.

528

529 Despite the channel being filled with sediment in the reconstructed bathymetry in the MLQ experiment we  
530 find an ice streaming pattern similar to that of the reference model, with even higher sliding in the outer parts  
531 of the Norwegian Channel from 23-17 ka near the shelf break because of the faster advance in the North Sea  
532 in this experiment. In the PREQ experiment streaming is limited to a pattern across channel towards the west  
533 because of the sediment wedge sloping along the shoreline leading the ice towards the middle North Sea. We  
534 find it likely that the channel could initially have been formed during multiple glacial periods since ~0.5 Ma  
535 before the main formation occurred in recent glacial periods (~0.35 Ma; Løseth et al. 2022). This would be in  
536 agreement with studies on the North Sea Fan (NCIS depocenter), suggesting that 90% of the sediments in this  
537 fan are younger than 0.5 Ma (Hjelstuen et al., 2012).

538

### 539 **5. Conclusion**

540 We have used a higher-order ice sheet model to investigate the effect of landscape morphology on the SIS  
541 evolution and dynamics. Three different experiments were conducted: (i) a reference experiment resembling  
542 the last glacial cycle using modern-day topography and bathymetry, (ii) a mid-late-Quaternary (MLQ)  
543 experiment with glacial morphological features in the present-day bathymetry filled with sediment, and (iii) a  
544 pre-Quaternary (PREQ) experiment, simulating the SIS on a reconstructed pre-glacial topography and  
545 bathymetry. We find in the MLQ experiment that removing glacial morphological features in the bathymetry  
546 allows for faster and further southward expansion at similar climatic conditions allowing for a larger ice sheet.  
547 On the contrary we find in the PREQ experiment that the early Quaternary bathymetry did not allow for the  
548 SIS to advance as far westward, thereby limiting the size of early glaciations and preventing a merge between  
549 the BIIS and the SIS. Looking at the prominent glacio-morphological feature, the Norwegian Channel, we find  
550 that the PREQ experiment do not allow for significant ice streaming in this area and that the channel was more  
551 likely formed since ~0.5 Ma. Furthermore, our results suggest ice streaming occurred in distinct stages along  
552 the trunk of the channel with high ice sliding in the inner parts before LGM and sliding in the outer parts of  
553 the channel close to the shelf break during LGM. Our results also show that sliding in the inner parts of the  
554 channel deactivated because of divergent ice flow when the BIIS and the SIS merged and formed a saddle  
555 across the North Sea.

556

### 557 **6. Code/Data availability**

558 Code and/or data will be made available upon request.



559 **7. Author contribution**

560 Gustav Jungdal-Olesen: Conceptualization, Methodology, Software, Formal analysis, Writing, original draft,  
561 Visualization. Vivi K. Pedersen: Conceptualization, Methodology, Supervision, Writing, review & editing,  
562 Funding acquisition. Jane L. Andersen: Writing, review & editing, Visualization. Andreas Born: Resources,  
563 Writing, review & editing

564

565 **8. Competing interests**

566 The authors declare that they have no conflict of interest.

567

568 **9. References**

569

570 Anderson, R. S., Dühnforth, M., Colgan, W. & Anderson, L. Far-flung moraines: Exploring the feedback of  
571 glacial erosion on the evolution of glacier length. *Geomorphology* 179, 269–285 (2012).

572

573 Bart, P.J., Mullally, D., Golledge, N.R., 2016. The influence of continental shelf bathymetry on  
574 antarctic ice sheet response to climate forcing. *Global and Planetary Change* 142, 87–95. URL:  
575 <http://dx.doi.org/10.1016/j.gloplacha.2016.04.009>, doi:10.1016/j.gloplacha.2016.04.009.

576

577 Batchelor, C.L., Margold, M., Krapp, M., Murton, D.K., Dalton, A.S., Gibbard, P.L., Stokes, C.R., Murton,  
578 J.B., Manica, A., 2019. The configuration of northern hemisphere ice sheets through the Quaternary. *Nature*  
579 *Communications* 10, 3713. URL: <http://www.nature.com/articles/s41467-019-11601-2>, doi:10.1038/s41467-  
580 019-11601-2.

581

582 Binzer, K., Stockmarr, J., Lykke-Andersen, H., 1994. Pre-Quaternary Surface Topography of Denmark.  
583 Geological Survey of Denmark map series no. 44.

584

585 Bondzio, J.H., Morlighem, M., Seroussi, H., Kleiner, T., Rückamp, M., Mouginit, J., Moon, T., Larour, E.Y.,  
586 Humbert, A., 2017. The mechanisms behind Jakobshavn Isbræ's acceleration and mass loss: A 3-D  
587 thermomechanical model study. *Geophysical Research Letters* 44, 6252–6260. doi:10.1002/2017GL073309.

588

589 Boulton, G., Hagdorn, M., 2006. Glaciology of the British Isles ice sheet during the last glacial cycle: form,  
590 flow, streams and lobes. *Quaternary Science Reviews* 25, 3359–3390. doi:10.1016/j.quascirev.2006.10.013.

591

592 Clague, J.J., Barendregt, R.W., Menounos, B., Roberts, N.J., Rabassa, J., Martinez, O., Ercolano, B., Corbella,  
593 H., Hemming, S.R., 2020. Pliocene and early Pleistocene glaciation and landscape evolution on the Patagonian  
594 steppe, Santa Cruz province, Argentina. *Quaternary Science Reviews* 227, 105992.  
595 doi:<https://doi.org/10.1016/j.quascirev.2019.105992>.

596



- 597 Cook, S.J., Swift, D.A., Kirkbride, M.P., Knight, P.G., Waller, R.I., 2020. The empirical basis for modelling  
598 glacial erosion rates. *Nature Communications* 11. doi:10.1038/s41467-020-14583-8.  
599
- 600 Dee, D., National Center for Atmospheric Research Staff (Eds). Last modified 2022-11-07 iThe Climate Data  
601 Guide: ERA-Interim. Retrieved from <https://climatedataguide.ucar.edu/climate-data/era-interim>  
602 on 2023-08-27.  
603
- 604 Dowdeswell, J.A., Ottesen, D., 2013. Buried iceberg ploughmarks in the early quaternary sediments of the  
605 central north sea: A two-million year record of glacial influence from 3d seismic data. *Marine Geology* 344,  
606 1ñ9. URL: <http://dx.doi.org/10.1016/j.margeo.2013.06.019>, doi:10.1016/j.margeo.2013.06.019.  
607
- 608 Egholm, D.L., Jansen, J.D., BrÊdstrup, C.F., Pedersen, V.K., Andersen, J.L., Ugelvig, S.V., Larsen, N.K.,  
609 Knudsen, M.F., 2017. Formation of plateau landscapes on glaciated continental margins. *Nature Geoscience*  
610 10, 592ñ597. doi:10.1038/NGEO2980.  
611
- 612 Egholm, D.L., Knudsen, M.F., Clark, C.D., Lesemann, J.E., 2011. Modeling the flow of glaciers in steep  
613 terrains: The integrated second-order shallow ice approximation (isosia). *Journal of Geophysical Research:*  
614 *Earth Surface* 116, 1ñ16. doi:10.1029/2010JF001900.  
615
- 616 Egholm, D.L., Nielsen, S.B., Pedersen, V.K., Lesemann, J.E., 2009. Glacial effects limiting mountain height.  
617 *Nature* 460, 884ñ887. doi:10.1038/nature08263.  
618
- 619 Egholm, D.L., Pedersen, V.K., Knudsen, M.F., Larsen, N.K., 2012a. Coupling the flow of ice, wa-  
620 ter, and sediment in a glacial landscape evolution model. *Geomorphology* 141-142, 47ñ66. URL:  
621 <http://dx.doi.org/10.1016/j.geomorph.2011.12.019>, doi:10.1016/j.geomorph.2011.12.019.  
622
- 623 Egholm, D.L., Pedersen, V.K., Knudsen, M.F., Larsen, N.K., 2012b. On the importance of  
624 higher order ice dynamics for glacial landscape evolution. *Geomorphology* 141-142, 67ñ80. URL:  
625 <http://dx.doi.org/10.1016/j.geomorph.2011.12.020>, doi:10.1016/j.geomorph.2011.12.020.  
626
- 627 Ewing, M., Donn, W.L., 1956. A theory of ice ages. *Science* 123, 1061–1066.  
628 doi:10.1126/science.123.3207.1061.  
629
- 630 GEBCO Bathymetric Compilation Group 2022., 2022. The GEBCO\_2022 Grid - a continuous terrain model  
631 of the global oceans and land. NERC EDS British Oceanographic Data Centre NOC. doi:10.5285/e0f0bb80-  
632 ab44-2739-e053-6c86abc0289c  
633



- 634 Gladstone, R., Moore, J., Wolovick, M., and Zwinger, T.: Sliding conditions beneath the Antarctic Ice Sheet,  
635 EGU General Assembly 2020, Online, 4–8 May 2020, EGU2020-7038, [https://doi.org/10.5194/egusphere-](https://doi.org/10.5194/egusphere-egu2020-7038)  
636 [egu2020-7038](https://doi.org/10.5194/egusphere-egu2020-7038), 2020
- 637
- 638 Goledowski, B., Nielsen, S.B., Clausen, O.R., 2012. Patterns of cenozoic sediment flux from western  
639 scandinavia. *Basin Research* 24, 377–400. doi:10.1111/j.1365-2117.2011.00530.x.
- 640
- 641 Hall, A.M., Ebert, K., Kleman, J., Nesje, A., Ottesen, D., 2013. Selective glacial erosion on the norwegian  
642 passive margin. *Geology* 41, 1203–1206. doi:10.1130/G34806.1.
- 643
- 644 Han, H.K., Gomez, N., Pollard, D., DeConto, R., 2021. Modeling northern hemispheric ice sheet dynamics,  
645 sea level change, and solid earth deformation through the last glacial cycle. *Journal of Geophysical Research:*  
646 *Earth Surface* 126, 1–15. doi:10.1029/2020JF006040.
- 647
- 648 Hjelstuen, B.O., Nygard, A., Sejrup, H.P., Hafliðason, H., 2012. Quaternary denudation of southern fennoscandia -  
649 evidence from the marine realm. *Boreas* 41, 379–390. doi:10.1111/j.1502-3885.2011.00239.x.
- 650
- 651 Houmark-Nielsen, M., 2004. The Pleistocene of Denmark: a review of stratigraphy and glaciation history. pp.  
652 35–46. URL: <https://linkinghub.elsevier.com/retrieve/pii/S1571086604800551>, doi:10.1016/S1571-  
653 0866(04)80055-1.
- 654
- 655 Hughes, A.L., Gyllencreutz, R., Øystein S. Lohne, Mangerud, J., Svendsen, J.I., 2016. The last  
656 eurAsian ice sheets - a chronological database and time-slice reconstruction, dated-1. *Boreas* 45, 1–45.  
657 doi:10.1111/bor.12142.
- 658
- 659 Hughes, P.D., Gibbard, P.L., 2018. Global glacier dynamics during 100 ka pleistocene glacial  
660 cycles. *Quaternary Research (United States)* 90, 222–243. doi:10.1017/qua.2018.37.
- 661
- 662 Hughes, T., Denton, G.H., Grosswald, M., 1977. Was there a late-wiirm arctic ice sheet? *Nature* 266, 596–  
663 602. doi:<https://doi.org/10.1038/266596a0>.
- 664
- 665 Jakobsson, M., Nilsson, J., Anderson, L., Backman, J., Björk, G., Cronin, T.M., Kirchner, N., Koshurnikov,  
666 A., Mayer, L., Noormets, R., O'Regan, M., Stranne, C., Ananiev, R., Macho, N.B., Cherniykh, D., Coxall, H.,  
667 Eriksson, B., Floden, T., Gemery, L., Orjan Gustafsson, Jerraegan, M., Stranne, C., Ananiev, R., Macho, N.B.,  
668 Cherniykh, D., Coxall, H., Eriksson, B., Floden, T., Gemery, L., Orjan Gustafsson, Jerram m, K., Johansson, C.,  
669 Khortov, A., Mohammad, R., Semiletov, I., 2016. Evidence for an ice shelf covering the central arctic ocean  
670 during the penultimate glaciation. *Nature Communications* 7. doi:10.1038/ncomms10365.
- 671



- 672 Japsen, P., Green, P.F., Chalmers, J.A., Bonow, J.M., 2018. Mountains of southernmost norway: Uplifted  
673 miocene peneplains and re-exposed mesozoic surfaces. *Journal of the Geological Society* 175, 721–741.  
674 doi:10.1144/jgs2017-157.
- 675
- 676 Jungclaus, J., Mikolajewicz, U., Kapsch, M.L., DiAgostino, R., Wieners, K.H., Giorgetta, M., Reick, C.,  
677 Esch, M., Bittner, M., Legutke, S., Schupfner, M., Wachsmann, F., Gayler, V., Haak, H., de Vrese, P.,  
678 Raddatz, T., Mauritsen, T., von Storch, J.S., Behrens, J., Brovkin, V., Claussen, M., Crueger, T., Fast, I.,  
679 Fiedler, S., Hagemann, S., Hohenegger, C., Jahns, T., Kloster, S., Kinne, S., Lasslop, G., Kornblueh, L.,  
680 Marotzke, J., Matei, D., Meraner, K., Modali, K., Mgemann, S., Hohenegger, C., Jahns, T., Kloster, S., Kinne,  
681 S., Lasslop, G., Kornblueh, L., Marotzke, J., Matei, D., Meraner, K., Modali, K., Müller, W., Nabel, J., Notz,  
682 D., Peters-von Gehlen, K., Pincus, R., Pohlmann, H., Pongratz, J., Rast, S., Schmidt, H., Schnur, R.,  
683 D., Peters-von Gehlen, K., Pincus, R., Pohlmann, H., Pongratz, J., Rast, S., Schmidt, H., Schnur, R.,  
684 Schulzweida, U., Six, K., Stevens, B., Voigt, A., Roeckner, E., 2019. Mpi-m mpi-esm1.2-lr model output  
685 prepared for cmip6 pmip lgm. URL: <https://doi.org/10.22033/ESGF/CMIP6.6642>,  
686 doi:10.22033/ESGF/CMIP6.6642
- 687
- 688 Kaplan, M. R., Hein, A. S., Hubbard, A. & Lax, S. M. Can glacial erosion limit the extent of glaciation?  
689 *Geomorphology* 103, 172–179 (2009).
- 690
- 691 Kessler, M.A., Anderson, R.S., Briner, J.P., 2008. Fjord insertion into continental margins driven by  
692 topographic steering of ice. *Nature Geoscience* 1, 365–369. doi:10.1038/ngeo201.
- 693
- 694 Lamb, R.M., Harding, R., Huuse, M., Stewart, M., Brocklehurst, S.H., 2018. The early quaternary north sea  
695 basin. *Journal of the Geological Society* 175, 275–290. doi:10.1144/jgs2017-057.
- 696
- 697 Liakka, J., Lofverstrom, M., Colleoni, F., 2016. The impact of the north american glacial topography on the  
698 evolution of the eurasian ice sheet over the last glacial cycle. *Climate of the Past* 12, 1225–1241.  
699 doi:10.5194/cp-12-1225-2016.
- 700
- 701 Lidmar-Bergstrom, K., Ollier, C.D., Sulebak, J.R., 2000. Landforms and uplift history of southern norway.  
702 *Global and Planetary Change* 24, 211–231. doi:10.1016/S0921-8181(00)00009-6.
- 703
- 704 Lindstrom, D.R., MacAyeal, D.R., 1986. Paleoclimatic constraints on the maintenance of possible ice-shelf  
705 cover in the Norwegian and Greenland seas. *Paleoceanography* 1, 313–337.  
706 doi:<https://doi.org/10.1029/PA001i003p00313>.
- 707
- 708 Lisiecki, L.E., Raymo, M.E., 2005. A pliocene-pleistocene stack of 57 globally distributed benthic 18o records.  
709 *Paleoceanography* 20, 1–17. doi:10.1029/2004PA001071.



- 710  
711 Løseth, H., Nygard, A., Batchelor, C.L., Fayzullaev, T., 2022. A regionally consistent 3d seismic-stratigraphic  
712 framework and age model for the quaternary sediments of the northern north sea. *Marine and Petroleum*  
713 *Geology* 142, 105766. doi:10.1016/j.marpetgeo.2022.105766.  
714  
715 MacGregor, K.R., Anderson, R.S., Waddington, E.D., 2009. Numerical modeling of glacial erosion and  
716 headwall processes in alpine valleys. *Geomorphology* 103, 189–204. doi:10.1016/j.geomorph.2008.04.022  
717  
718 Magrani, F., Valla, P.G., Egholm, D., 2022. Modelling alpine glacier geometry and subglacial erosion pat-  
719 terns in response to contrasting climatic forcing. *Earth Surface Processes and Landforms* 47, 1054–1072.  
720 doi:10.1002/esp.5302.  
721  
722 Mas e Braga, M., Jones, R.S., Bernales, J. et al. A thicker Antarctic ice stream during the mid-Pliocene warm  
723 period. *Commun Earth Environ* 4, 321 (2023). <https://doi.org/10.1038/s43247-023-00983-3>  
724  
725 Millan, R., Mouginit, J., Rabatel, A., Morlighem, M., 2022. Ice velocity and thickness of the world's glaciers.  
726 *Nature Geoscience* 15, 124–129. doi:10.1038/s41561-021-00885-z.  
727  
728 Millstein, J.D., Minchew, B.M., Pegler, S.S., 2022. Ice viscosity is more sensitive to stress than commonly  
729 assumed. *Communications Earth and Environment* 3. doi:10.1038/s43247-022-00385-x.  
730  
731 Nielsen, T., Mathiesen, A., Bryde-Auken, M., 2008. Base quaternary in the danish parts of the north sea and  
732 skagerrak. *Geological Survey of Denmark and Greenland Bulletin* , 37–40doi:10.34194/geusb.v15.5038.  
733  
734 Olsen, L., Sveian, H., Ottesen, D., Rise, L., 2013. Quaternary glacial, interglacial and interstadial deposits of  
735 norway and adjacent onshore and offshore areas. *Geological Survey of Norway Special Publication* 13.  
736  
737 Patton, H., Hubbard, A., Andreassen, K., Winsborrow, M., Stroeven, A.P., 2016. The build-up, configuration,  
738 and dynamical sensitivity of the eurasian ice-sheet complex to late weichselian climatic and oceanic forcing.  
739 *Quaternary Science Reviews* 153, 97–121. URL: <http://dx.doi.org/10.1016/j.quascirev.2016.10.009>,  
740 doi:10.1016/j.quascirev.2016.10.009.  
741  
742 Patton, H., Hubbard, A., Heyman, J., Alexandropoulou, N., Lasabuda, A., Stroeven, A.P., 2022. The profound  
743 yet transient nature of glacial erosion , 1–38doi:10.1038/s41467-022-35072-0.  
744  
745 Pedersen, V.K., Huisman, R.S., Herman, F., Egholm, D.L., 2014. Controls of initial topography on temporal  
746 and spatial patterns of glacial erosion. *Geomorphology* 223, 96–116. URL:  
747 <http://dx.doi.org/10.1016/j.geomorph.2014.06.028>, doi:10.1016/j.geomorph.2014.06.028





- 748  
749 Pedersen, V.K., Huismans, R.S., Moucha, R., 2016. Isostatic and dynamic support of high topography on a  
750 north atlantic passive margin. *Earth and Planetary Science Letters* 446, 1ñ9. URL:  
751 <http://dx.doi.org/10.1016/j.epsl.2016.04.019>, doi:10.1016/j.epsl.2016.04.019.  
752  
753 Pedersen, V.K., Knutsen, Å. K., Pallisgaard-Olesen, G., Andersen, J.L., Moucha, R., Huismans, R.S., 2021.  
754 Widespread glacial erosion on the scandinavian passive margin. *Geology Early Publ*, 1ñ5.  
755 doi:10.1130/G48836.1/5304547/g48836.pdf.  
756  
757 Pendergrass, A., Wang, J., National Center for Atmospheric Research Staff (Eds). Last modified 2022-11-07  
758 "The Climate Data Guide: GPCP (Monthly): Global Precipitation Climatology Project." Retrieved from  
759 <https://climatedataguide.ucar.edu/climate-data/gpcp-monthly-global-precipitation-climatology-project>  
760 on 2023-09-03.  
761  
762 Rea, B.R., Newton, A.M.W., Lamb, R.M., Harding, R., Bigg, G.R., Rose, P., Spagnolo, M., Huuse, M., Cater,  
763 J.M.L., Archer, S., Buckley, F., Halliyeva, M., Huuse, J., Cornwell, D.G., Brocklehurst, S.H., Howell, J.A.,  
764 2018. Extensive marine-terminating ice sheets in europe from 2.5 million years ago. *Science Advances* 4,  
765 eaar8327. doi:10.1126/sciadv.aar8327.  
766  
767 Rise, L., Ottesen, D., Berg, K., Lundin, E., 2005. Large-scale development of the mid-norwegian margin  
768 during the last 3 million years. *Marine and Petroleum Geology* 22, 33ñ44.  
769 doi:10.1016/j.marpetgeo.2004.10.010.  
770  
771 Sejrup, H.P., Clark, C.D., Hjelstuen, B.O., 2016. Rapid ice sheet retreat triggered by ice stream debuitressing:  
772 Evidence from the north sea. *Geology* 44, 355ñ358. doi:10.1130/G37652.1.  
773  
774 Sejrup, H.P., Landvik, J.Y., Larsen, E., Janockom, J., Eiriksson, J., King, E., 1998. The jf fren area, a border  
775 zone of the norwegian channel ice stream.  
776  
777 Sejrup, H.P., Larsen, E., Haflidason, H., Berstad, I.M., Hjelstuen, B.O., Jonsdottir, H.E., King, E.L., Landvik,  
778 J., Longva, O., Nygard, A., Ottesen, D., Raunholm, S., Rise, L., Stalsberg, K., 2003. Configuration, history  
779 and impact of the norwegian channel ice stream. *Boreas* 32, 18ñ36. doi:10.1080/03009480310001029.  
780  
781 Simms, A.R., Lisiecki, L., Gebbie, G., Whitehouse, P.L., Clark, J.F., 2019. Balancing the last glacial maximum  
782 (lgm) sea-level budget. *Quaternary Science Reviews* 205, 143ñ153. doi:10.1016/j.quascirev.2018.12.018.  
783



- 784 Steer, P., Huismans, R.S., Valla, P.G., Gac, S., Herman, F., 2012. Recent glacial erosion of fjords and low-  
785 relief surfaces in western scandinavia. Nature Geoscience 14, 4433. URL: <http://dx.doi.org/10.1038/ngeo1549>,  
786 doi:<http://www.nature.com/ngeo/journal/v5/n9/abs/ngeo1549.html#supplementary-information>.  
787  
788 Wickert, A. D. (2016), Open-source modular solutions for flexural isostasy: gFlex v1.0, Geosci. Model Dev.,  
789 9(3), 997–1017, doi:10.5194/gmd-9-997-2016.